Letter

A Range-Based Node Localization Scheme for UWASNs Considering Noises and Aided With Neurodynamics Model

Lijuan Wang, Xiujuan Du, and Chong Li

Dear Editor,

This letter focuses on the node localization problem in underwater acoustic sensor networks (UWASNs) with the time-dependent property and various noise disturbances. A range-based localization scheme aided with an integral-feedback-based neurodynamics (IND) model is proposed and referred to as IND-RS, which has the stability against the internal perturbations encountered during the solving process. Considering the complexity of the underwater environment, the Kalman filter (KF) algorithm is smoothly integrated into IND-RS to well eliminate environmental noises to improve the localization accuracy. Besides, the convergence analyses and robustness proofs on the proposed IND model are furnished. Extensive simulations in different localization scenarios are conducted to substantiate the superiority of IND-RS in terms of high accuracy and strong stability.

In UWASNs [1], [2], localization is a fundamental and critical technology. Range-based schemes from the time difference of arrival (TDoA) measurement provide a high localization precision and become the preferred option for UWASNs. For instance, in [3], by utilizing TDoA measurements, a non-convex and partially observable solution is presented for underwater vehicle localization. Besides, Sun *et al.* [4] construct a second-order TDoA algorithm to address the problem of signal drift. In [5], a TDoA-based prediction localization algorithm is designed to achieve high accuracy and energy efficiency.

Although extensive achievements have been gained by the above researches, the schemes therein still have limitations. First, due to the complexity of the underwater environment [6], TDoA measurements obtained from the natural world are mingled with bias, which grossly decreases the localization accuracy, but was not raised in these studies. In addition, given that the node may move passively or in a controlled manner, the localization problem in UWASN is essentially time-dependent, which indicates that static schemes would introduce lagging errors due to the lack of time derivative information of dynamic parameters.

It has been verified that the zeroing neurodynamics methodology which is originated from the recurrent neural network (RNN), is qualified for dealing with a variety of mathematical and engineering problems [7], [8]. Therefore, owing to the efficient real-time computation ability, an IND model is proposed for the node localization in this letter. Furthermore, given the fact of the inevitable perturbations during the solving process and inspired by the noise-tolerance mechanism in cybernetics, an integral-feedback term is incorporated into the proposed IND model to effectively offset the perturbation error.

Corresponding author: Xiujuan Du.

The authors are with the School of Computer, Qinghai Normal University, Qinghai Provincial Key Laboratory of IoT, Xining 810008, the State Key Laboratory of Tibetan Intelligent Information Processing and Application, Xining 810008, and Academy of Plateau Science and Sustainability, Xining 810008, China (e-mail: 1041517271@qq.com; dxj@qhnu.edu.cn; 1055143986@qq.com).

In addition, the KF algorithm is introduced to weaken the impact of environmental noises and improve the accuracy of TDoA measurements [4]. Hence, the motivation of this letter is to construct a range-based node localization scheme in UWASNs from TDoA measurements with the capabilities of real-time computation and resistance to both environmental and internal noises and disturbances.

Problem formulation: Consider an underwater scenario in which a target moves along a trajectory and n neighboring anchors are randomly deployed and fixed, of which $n \geq 4$ for the 2-dimensional (2D) case and $n \geq 5$ for the 3-dimensional (3D) case. For the 3D case, the coordinates of n anchors and the target are defined as

$$
\mathcal{A}_{poi} = \begin{bmatrix} x_1 & x_2 & \dots & x_n \\ y_1 & y_2 & \dots & y_n \\ z_1 & z_2 & \dots & z_n \end{bmatrix} \in \mathbb{R}^{3 \times n}, \ \mathcal{T}_{poi} = \begin{bmatrix} x(t) \\ y(t) \\ z(t) \end{bmatrix} \in \mathbb{R}^3.
$$

According to the meaning of TDoA, we have the following equations:

$$
r_i(t) = \sqrt{(x_i - x(t))^2 + (y_i - y(t))^2 + (z_i - z(t))^2},
$$
$$
r_{i1}(t) = r_i(t) - r_1(t) = v \Delta T_{i1}(t), \ \ \Delta T_{i1}(t) = T_i(t) - T_1(t)
$$

where $i \in \{1, 2, \dots, n\}$; $r_i(t)$ represents the distance between the target and the ith anchor; $r_{i1}(t)$ denotes the distance difference from the target to the ith and first anchors; $T_i(t)$ stands for the time of the signal traveling from the target to the ith anchor; v is the propagation speed of acoustic signals; $\Delta T_{i1}(t)$ signifies the time difference of the signal traveling from the target to the ith and first anchors separately. By several derivations, the node localization problem from TDoA measurements in the 3D scenario is expressed as

$$
\begin{bmatrix} x_{21} & y_{21} & z_{21} & r_{21}(t) \\ x_{31} & y_{31} & z_{31} & r_{31}(t) \\ \vdots & \vdots & \vdots & \vdots \\ x_{n1} & y_{n1} & z_{n1} & r_{n1}(t) \end{bmatrix} \begin{bmatrix} x(t) \\ y(t) \\ z(t) \\ r_1(t) \end{bmatrix} = \begin{bmatrix} (\Lambda_{21} - r_{21}^2(t))/2 \\ (\Lambda_{31} - r_{31}^2(t))/2 \\ \vdots \\ (\Lambda_{n1} - r_{n1}^2(t))/2 \end{bmatrix} \quad (1)
$$

where $x_{i1} = x_i - x_1$, $y_{i1} = y_i - y_1$ and $z_{i1} = z_i - z_1$; $\Lambda_{n1} = \Lambda_n - \Lambda_1$ with $\Lambda_i = x_i^2 + y_i^2 + z_i^2$. From (1), it can be seen that the node localization problem using TDoA measurements in UWASNs is formulated as a dynamic matrix equation and concisely described as

$$
A(t) \boldsymbol{u}(t) = \boldsymbol{h}(t) \quad (2)
$$

where $A(t) \in \mathbb{R}^{(n-1) \times a}$, a known coefficient matrix with $n, a \in \mathbb{Z}$, involves TDoA measurements as well as the coordinates of anchors; $\boldsymbol{h}(t) \in \mathbb{R}^{n-1}$ is a known vector; $\boldsymbol{u}(t) \in \mathbb{R}^a$, an unknown vector with $a = 3$ or $a = 4$, is associated with the coordinate of the target to be determined.

Design of IND-RS: Firstly, IND-RS adopts the KF algorithm to filter TDoA measurements to compensate for the measured bias which can be deemed as an additive Gaussian white noise. Then, the filtered results would be the input of the proposed IND model to solve the node localization problem (2) and determine the position of the target.

Filtering of TDoA measurements: With the biased TDoA measurements, the core procedures of the KF algorithm are described as follows:

$$
\hat{\boldsymbol{x}}_{\varsigma, \varsigma-1} = A \hat{\boldsymbol{x}}_{\varsigma-1, \varsigma-1}
$$
$$
\boldsymbol{p}_{\varsigma, \varsigma-1} = A \boldsymbol{p}_{\varsigma-1, \varsigma-1} A^T + Q
$$
$$
K_\varsigma = \boldsymbol{p}_{\varsigma, \varsigma-1} H^T (H \boldsymbol{p}_{\varsigma, \varsigma-1} H^T + R)^{-1}
$$
$$
\hat{\boldsymbol{x}}_{\varsigma, \varsigma} = \hat{\boldsymbol{x}}_{\varsigma, \varsigma-1} + K_\varsigma (z_\varsigma - H \hat{\boldsymbol{x}}_{\varsigma, \varsigma-1})
$$
$$
\boldsymbol{p}_{\varsigma, \varsigma} = (I - K_\varsigma H) \boldsymbol{p}_{\varsigma, \varsigma-1}
$$

where superscript T denotes the transpose operator; $\varsigma \in \{1, 2, \dots, M\}$ is the iteration index of the KF; $\hat{\boldsymbol{x}}$ represents the estimate of TDoA measurements; z symbolizes the biased TDoA measurements; the definitions of I, K, A, Q, R and $\boldsymbol{p}$ are regular, thus omitted. After-

wards, $\hat{x}_{M,M}$ is used as the input to the following IND model.

IND model: IND model is proposed for solving the node localization problem (2) with high effectiveness and high accuracy.

First of all, a dynamic error function of (2) is defined as

$$e(t) = A(t)u(t) - h(t). \tag{3}$$

When $e(t)$ approaches zero, the obtained solution $u(t)$ approaches the theoretical solution $u^*(t)$. To this end, the evolution for $e(t)$ is designed as

$$\dot{e}(t) = -k_1 e(t) - k_2 \int_0^t e(\tau)d\tau \tag{4}$$

where parameters $k_1, k_2 > 0$ aiming at regulating the convergence rate of $\dot{e}(t)$ which denotes the derivative of $e(t)$. Further, by expanding (4), the proposed IND model is obtained

$$\dot{u}(t) = -A^\dagger(t)\Big(k_1(A(t)u(t) - h(t)) + \dot{A}(t)u(t) - \dot{h}(t) + k_2 \int_0^t (A(\tau)u(\tau) - h(\tau))d\tau\Big) \tag{5}$$

where $A^\dagger(t)$ denotes the pseudoinverse of matrix $A(t)$.

Theoretical analyses:

Convergence analyses: Theorem 1 provides the proof on the convergence of IND model (5) without perturbations.

Theorem 1: Starting from a random and less exact position $u(0)$, the estimate position $u(t)$ of the target, which is generated by IND model (5), globally converges to the theoretical position $u^*(t)$.

Proof: IND model (5) is generalized from $\dot{e}(t) = -k_1 e(t) - k_2 \int_0^t e(\tau)d\tau$ with the ith subsystem expressing as

$$\dot{e}_i(t) = -k_1 e_i(t) - k_2 \int_0^t e_i(\tau)d\tau \tag{6}$$

for $\forall i \in 1, \ldots, n-1$. Then, we define a Lyapunov function candidate for $\dot{e}_i(t)$

$$\mathcal{V}(t) = e_i^2(t) + k_2 \left(\int_0^t e_i(\tau)d\tau\right)^2. \tag{7}$$

The time derivative of $\mathcal{V}(t)$ is obtained as $\dot{\mathcal{V}}(t) = -2k_1 e_i^2(t)$. We have $\mathcal{V}(t) \geq 0$ and $\dot{\mathcal{V}}(t) \leq 0$. Based on the Lyapunov Theory, it can be concluded that $e_i(t)$ globally converges to zero. That is to say, the estimate position of the target, which is generated by IND model (5), globally converges to the theoretical position $u^*(t)$. ∎

Robustness analyses: Theorems 2 and 3 are provided to investigate the robustness of IND model (5) against constant and random perturbations, respectively, during the solving process of the node localization. To lay a basis for further investigation, the disturbed IND model is generated as follows:

$$\dot{u}(t) = A^\dagger(t)\Big(-k_1(A(t)u(t) - h(t)) - \dot{A}(t)u(t) + \dot{h}(t) - k_2 \int_0^t (A(\tau)u(\tau) - h(\tau))d\tau + \varrho(t)\Big) \tag{8}$$

where $\varrho(t) \in \mathbb{R}^{n-1}$ denotes the unknown perturbation encountered during the solving process, such as the constant implementation error, the random perturbations, or their superposition.

Theorem 2: When undergoing the constant perturbation $\varrho(t) = \varrho \in \mathbb{R}^{n-1}$ during the practical solving process of the node localization problem (2), the disturbed IND model (8) globally converges to the theoretical position of the target, i.e., the residual error $\|e(t)\|_2$ of the disturbed IND model (8) globally converges to zero.

Proof: By Laplace transform, the ith subsystem of the disturbed IND model (8) is deduced

$$se_i(s) - e_i(0) = -k_1 e_i(s) - \frac{k_2}{s} e_i(s) + \varrho_i(s) \tag{9}$$

then,

$$e_i(s) = \frac{s(e_i(0) + \varrho_i(s))}{s^2 + sk_1 + k_2} \tag{10}$$

with the transfer function $s/(s^2 + sk_1 + k_2)$, of which the poles are $s_1 = (-k_1 + \sqrt{k_1^2 - 4k_2})/2$ and $s_2 = (-k_1 - \sqrt{k_1^2 - 4k_2})/2$. For $k_1, k_2 > 0$, it can be concluded that both s_1 and s_2 locate on the left-half plane of s, which implies this system is stable theoretically. The constant

noise amounts to a step signal disturbance input term with the Laplace transform $\varrho_i(s) = \bar{\varrho}_i/s$. Therefore, using the final value theorem, it can be acquired that

$$\lim_{t \to \infty} e_i(t) = \lim_{s \to 0} se_i(s) = \lim_{s \to 0} \frac{s^2(e_i(0) + \bar{\varrho}_i/s)}{s^2 + sk_1 + k_2} = 0. \tag{11}$$

Thus, it can be concluded that $\lim_{t \to \infty} \|e(t)\|_2 = 0$ under the constant perturbation. ∎

Theorem 3: When undergoing a bounded random perturbation $\varrho(t) \in \mathbb{R}^{n-1}$ during the practical solving process of the node localization problem (2), the disturbed IND model (8) globally converges to the theoretical position with a bounded residual error $\|e(t)\|_2$.

Proof: The disturbed IND model (8) is generalized from $\dot{e}(t) = -k_1 e(t) - k_2 \int_0^t e(\tau)d\tau + \varrho(t)$ with the ith subsystem expressing as

$$\dot{e}_i(t) = -k_1 e_i(t) - k_2 \int_0^t e_i(\tau)d\tau + \varrho_i(t) \tag{12}$$

for $\forall i = 1, \ldots, n-1$.

Depending on the values of k_1 and k_2, we continue the discussion from the following three situations:

1) For $k_1^2 > 4k_2$, the solution to (12) is

$$e_i(t) = \frac{e_i(0)(\beta\exp(\beta t) - \theta\exp(\theta t))}{\beta - \theta} + \Big(\int_0^t \big(\beta\exp(\beta(t-\tau)) - \theta\exp(\theta(t-\tau))\big)\varrho_i(\tau)d\tau\Big)\frac{1}{\beta - \theta} \tag{13}$$

where $\beta = (-k_1 + \sqrt{k_1^2 - 4k_2})/2$, $\theta = (-k_1 - \sqrt{k_1^2 - 4k_2})/2$. Subsequently, in terms of the triangle inequality, the above equation can be turned into

$$|e_i(t)| \leq \Big(|e_i(0)(\beta\exp(\beta t) - \theta\exp(\theta t))| + \int_0^t |\beta\exp(\beta(t-\tau))|\|\varrho_i(\tau)|d\tau + \int_0^t |\theta\exp(\theta(t-\tau))|\|\varrho_i(\tau)|d\tau\Big)\frac{1}{\beta - \theta}.$$

We further have

$$|e_i(t)| \leq \Big(e_i(0)(\beta\exp(\beta t) - \theta\exp(\theta t)) + 2\max_{0 \leq \tau \leq t}|\varrho_i(\tau)|\Big)\frac{1}{\sqrt{\beta - \theta}}.$$

As a result, it can be derived that

$$\sup_{t \to \infty} \|e(t)\|_2 \leq \frac{2\bar{\varrho}\sqrt{n-1}}{\sqrt{k_1^2 - 4k_2}}$$

of which $n \geq 4$, $\bar{\varrho} = \max_{0 \leq \tau \leq t}\{\max_{3 \leq i \leq n-1}|\varrho_i(\tau)|\}$.

2) For $k_1^2 < 4k_2$, similar derivations can deduce that

$$\sup_{t \to \infty} \|e(t)\|_2 \leq \frac{4k_2\bar{\varrho}\sqrt{n-1}}{k_1\sqrt{k_1^2 - 4k_2}}.$$

3) For $k_1^2 = 4k_2$, similarly, we have

$$\sup_{t \to \infty} \|e(t)\|_2 \leq \Big(\frac{\iota}{\omega} - \frac{1}{\beta}\Big)\bar{\varrho}\sqrt{n-1}$$

with ι, ω being positive values. ∎

Experiments: In this part, the true path of the target node is signified by TP, and the estimated path is signified by estimated path (EP).

2D/3D: It can be seen from Fig. 1(a) that, in a 0.2 km × 0.2 km area, the target moves along a curved path from point A to point B, and the estimated path generated by IND-RS well coincides with the curve. Also, as visualized in Fig. 1(b), the residual error $\|e(t)\|_2$ converges at $t = 2$ s with the order of 10^{-1} for both the constant perturbation $\varrho(t) = [5]^{6 \times 1}$ and the random perturbation $\varrho(t) \in [4,6]^{6 \times 1}$. Moreover, the convergence of the residual errors $\|e(t)\|_2$ with four initial values in the case of no perturbation is presented in Figs. 1(c) and 1(d). The convergent rate of the residual error $\|e(t)\|_2$ with $k_1 = k_2 = 5$ shown in Fig. 1(c) is smaller than that with $k_1 = k_2 = 15$ shown in Fig. 1(d).

For a 3D scenario with the range of 0.2 km × 0.2 km × 60 m shown in Fig. 2(a), IND-RS is capable of quickly locating the target
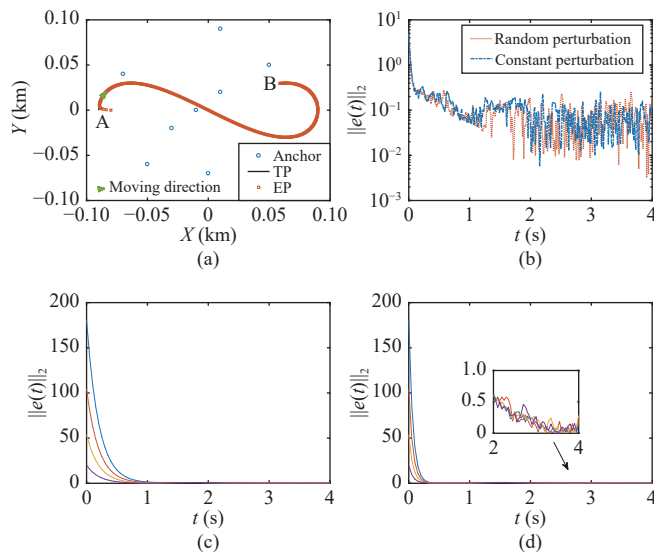
Fig. 1. Validation results of the node localization using IND-RS under different perturbation workspaces in the 2D scenario. (a) TP and EP; (b) Residual error $\|e(t)\|_2$ with $\varrho(t) = [5]^{6\times1}$ and $\varrho(t) \in [4,6]^{6\times1}$; (c) Residual error $\|e(t)\|_2$ with $k_1 = 5$ and $k_2 = 5$ under the zero perturbation workspace; (d) Residual error $\|e(t)\|_2$ with $k_1 = 15$ and $k_2 = 15$ under the zero perturbation workspace.
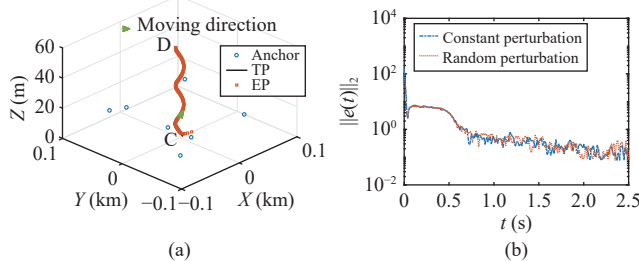

Fig. 2. Validation results of the node localization using IND-RS under different perturbation workspaces in the 3D scenario. (a) TP and EP; (b) Residual error $\|e(t)\|_2$ with $\varrho(t) = [5]^{4\times1}$ and $\varrho(t) \in [4,6]^{4\times1}$.

from a rough and initial position $[0.05; 0; 0]$ km and tracking it accurately. As depicted in Fig. 2(b), the residual error $\|e(t)\|_2$ converges within 2 s for both the constant perturbation $\varrho(t) = [5]^{6\times1}$ and the random perturbation $\varrho(t) \in [4,6]^{6\times1}$.

Comparative results: For comparison, the disturbed model without the integral term is given as follows:

$$\dot{u}(t) = A^{\dagger}(t)(-k_1(A(t)u(t) - h(t)) - \dot{A}(t)u(t) + \dot{h}(t) + \varrho(t)). \quad (14)$$

Obviously, the path estimated by the model (14) in Fig. 3(a) is deviated from the true path when compared with paths estimated by IND mode (8) shown in Figs. 3(b) and 3(c). However, as shown in Figs. 3(b) and 3(c), a few of fluctuations are observed in the process of locating the target. As a further exploration, two anchors are added into the scenario. Fig. 3(d) shows that the estimated path generated by IND model (8) with the aid of 7 anchors is perfectly completed. From this result, it can be concluded that an appropriate distribution of the anchors can contribute to the localization accuracy of the proposed IND-RS scheme.

Conclusion: This letter has investigated the node localization problem in UWASNs from a dynamic perspective. Given that the underwater environment is fragile and complicated, the KF algo-
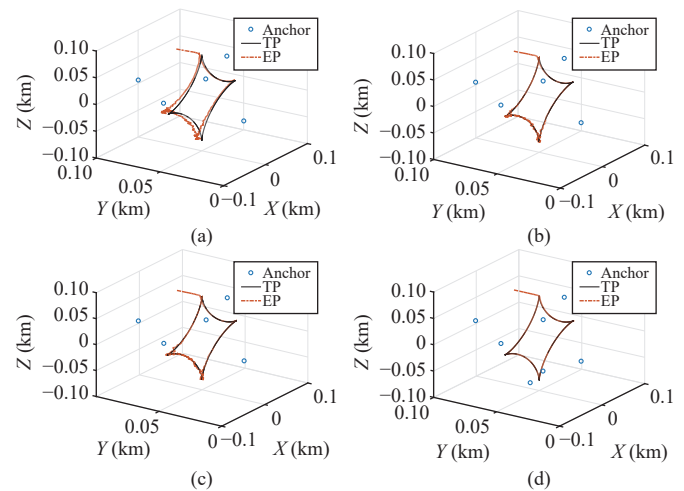

Fig. 3. Comparative results of the node localization using model (14) and IND model (8) to aid IND-RS under different perturbation workspaces in the 3D scenario. (a) TP and EP of model (14) with $\varrho(t) = [5]^{4\times1}$ and $n = 5$; (b) TP and EP of IND model (8) with $\varrho(t) = [5]^{4\times1}$ and $n = 5$; (c) TP and EP of IND model (8) with $\varrho(t) \in [4,6]^{4\times1}$ and $n = 5$; (d) TP and EP of IND model (8) with $\varrho(t) = [5]^{6\times1}$ and $n = 7$.

rithm and IND model (5) have been employed to establish a new range-base scheme, i.e., IND-RS, with high accuracy and strong stability. Rigorous theoretical analyses and simulative experiments have been provided to verify the effectiveness and feasibility of IND-RS for node localization in the presence of various kinds of noise or perturbations.

References

[1] J. Partan, J. Kurose, and B. Levine, "A survey of practical issues in underwater networks," in *Proc. ACM Int. Workshop Underw. Netw.*, 2006, pp. 17–24.

[2] J. Zheng and A. Jamalipour, *Wireless Sensor Networks: A Networking Perspective*, Hoboken, USA: John Wiley & Sons, 2009.

[3] T. Alexandri, M. Walter, and R. Diamant, "A time difference of arrival based target motion analysis for localization of underwater vehicles," *IEEE Trans. Veh. Technol.*, vol. 71, no. 1, pp. 326–338, Jan. 2022.

[4] S. Sun, S. Qin, Y. Hao, G. Zhang, and C. Zhao, "Underwater acoustic localization of the black box based on generalized second-order time difference of arrival (GSTDOA)," *IEEE Trans. Geosci. Remote Sens.*, vol. 59, no. 9, pp. 7245–7255, Sept. 2021.

[5] W. Zhang, G. Han, X. Wang, M. Guizani, K. Fan, and L. Shu, "A node location algorithm based on bode movement prediction in underwater acoustic sensor networks," *IEEE Trans. Veh. Technol.*, vol. 69, no. 3, pp. 3166–3178, Mar. 2020.

[6] H. Zhao, J. Yan, X. Luo, and X. Gua, "Privacy preserving solution for the asynchronous localization of underwater sensor networks," *IEEE/CAA J. Autom. Sinica*, vol. 7, no. 6, pp. 1511–1527, Nov. 2020.

[7] J. Zhang, L. Jin, Y. Wang, and C. Yang, "A collaboration scheme for controlling multimanipulator system: A game-theoretic perspective," *IEEE/ASME Trans. Mechatron.*, vol. 28, no. 1, pp. 128–139, Feb. 2023.

[8] Z. Xie, L. Jin, and X. Luo, "Kinematics-based motion-force control for redundant manipulators with quaternion control," *IEEE Trans. Autom. Sci. Eng.*, vol. 20, no. 3, pp. 1815–1828, Jul. 2023.